Time-dependent spintronic anisotropy in magnetic molecules

Kacper Wrześniewski* and Ireneusz Weymann
Faculty of Physics, Adam Mickiewicz University, ul. Uniwersytetu Poznańskiego 2, 61-614 Poznań, Poland

(Received 6 April 2020; revised manuscript received 8 June 2020; accepted 9 June 2020; published 23 June 2020)

We theoretically study the quench dynamics of induced anisotropy of a large-spin magnetic molecule coupled to spin-polarized ferromagnetic leads. The real-time evolution is calculated by means of the time-dependent density-matrix numerical renormalization group method implemented within the matrix product states framework, which takes into account all correlations in a very accurate manner. We determine the system response to a quench in the spin-dependent coupling to ferromagnetic leads. In particular, we focus on the transient dynamics associated with crossing from the weak- to the strong-coupling regime, where the Kondo correlations become important. The dynamics is examined by calculating the time-dependent expectation values of the spin-quadrupole moment and the associated spin operators. We identify the relevant timescales describing the quench dynamics and determine the influence of the effective exchange coupling of molecules and spin polarization of the leads on the dynamical behavior of the system. Furthermore, the generalization of our predictions for large spin values of molecules is considered. Finally, we analyze the effect of finite temperature and show that it gives rise to a reduction of magnetic anisotropy by strong suppression of the time-dependent spin-quadrupole moment due to thermal fluctuations.

DOI: 10.1103/PhysRevB.101.245434

I. INTRODUCTION

Molecular magnetism is a rapidly developing area of theoretical and experimental research, providing concepts for novel applications in spintronic devices and quantum technologies [1–10]. Single-molecule magnets (SMM), in particular those of large spin ($S \geqslant 1$), are especially appealing due to their unique magnetic characteristics and a wide perspective of engineering and synthesizing new specimen with sought properties [3]. One prominent feature present in magnetic molecular systems is the uniaxial magnetic anisotropy, which leads to the magnetic bistability and suppression of spin-reversal processes [11–15]. It is a property of crucial importance for the memory storage and information processing applications. Additionally, when transverse anisotropy component is considerable, quantum tunneling of magnetization may occur [16–19]. The transport properties of magnetic molecules have already been extensively studied [20–31], including the influence of the Kondo effect [32–36] in the strong-coupling regime [37–43]. However, when the physics of SMM systems incorporates spintronics, new prominent effects are revealed, including switching with spin-polarized currents, the Berry-phase blockade, or spintronic anisotropy among many others [44–52]. In fact, the latter effect is of the particular interest, as it allows for generation of magnetic anisotropy in spin-isotropic molecules [53].

Moreover, the dynamics of molecular systems, an important aspect of the on-going research in molecular magnetism, has recently gained a lot of attention and has been explored both experimentally [54–56] and theoretically [57–60]. Thus broadening further the knowledge and understanding of transport and dynamical properties of large-spin molecules is important both because of exciting fundamental aspects as well as due to possible applications in modern nanoelectronics, spintronics, and quantum information.

Motivated by recent progress within this field, in this paper we investigate the dynamical behavior of a large-spin magnetic molecule attached to spin-polarized leads, with an emphasis on the buildup of quadrupolar exchange field, referred to as spintronic anisotropy. Commonly, the intrinsic magnetic anisotropy arises from the spin-orbit interaction. However, it has been shown that the ferromagnetic proximity effect [61–64] can generate significant magnetic anisotropy in molecular systems in form of an effective exchange field [53]. The advantage of this approach is the possibility to electrically control both the magnitude of the anisotropy and the spin state of the system. When the coupling strength to external contacts is varied, a rapid change in the magnetic properties of the system occurs [53,65]. In particular, the quadrupolar moment of molecules is significantly reduced, when the system is tuned from the weak- to the strong-coupling regime. This substantial change of the moment is due to the Kondo screening of the orbital level spin of the molecule and is a nontrivial many-body effect resulting from the interplay of magnetism and the Kondo physics. It was also shown experimentally that quadrupolar interaction in SMM systems has an important influence on tunneling dynamics [66]. In a real setup, tuning between the different coupling regimes can be achieved by electrically shifting the tunnel barriers with respective gates.

Considering all the above, we focus on the theoretical study of the quench dynamics of the spintronic quadrupole moment due to the Kondo correlations. In particular, we identify the universal timescale for the dynamics describing the quench

*wrzesniewski@amu.edu.pl

of spintronic anisotropy. Moreover, we examine the influence of the magnitude of effective exchange coupling, leads spin polarization, and the total spin of the molecule on discussed dynamical effects. Lastly, we also analyze the influence of finite temperature, showing that in certain range of temperatures, a strong suppression of magnetic properties is predicted. In pursuance of the precise analysis of the system response to the considered quench in the strong-coupling regime, we resort to the Wilson's numerical renormalization group (NRG) method [67–69]. We use the extended implementation allowing for studying the time evolution of the system, namely, the time-dependent numerical renormalization group (tNRG) [70–74]. This method allows for taking into account all the correlations in a fully nonperturbative manner and, thus, generating reliable predictions for the dynamics of the system under investigation.

This paper is structured as follows. Section II consists of the Hamiltonian description of the considered system, the overview of the quench protocol and a summary of the numerical renormalization group method used for calculations of time-dependent expectation values of local observables. In Sec. III, we present the numerical results and relevant analysis for the quantum quenches in the coupling strength from the weak to the strong-coupling regime. We also present and discuss the effects of finite temperature on dynamical behavior. Finally, the work is concluded in Sec. IV.

II. THEORETICAL FRAMEWORK

A. Hamiltonian

The effective spin Hamiltonian of a molecular magnet expressed only with spin coordinates can be written as

$$H_{\text{eff}} = BS_z + DQ_{zz}. \tag{1}$$

Here, S_z is the zth component of the total spin S, $Q_{zz} \equiv S_z^2 - S(S+1)/3$ is the zth diagonal tensor element of the spin-quadrupole moment, B is a dipolar field corresponding to external magnetic field, D is a quadrupolar field related to intrinsic spin-orbit interaction. This approximate approach is well-established for convenient description of the system spectrum and is often used to interpret the spectroscopic data [3]. In our considerations, however, the above-introduced quantities are generated purely by the spin-dependent coupling to ferromagnetic leads [53,62], which allows for tuning of both B and D by electrical means—the property that makes this approach advantageous from the application point of view.

In order to analyze the dynamical behavior of the system with tNRG and, especially, capture all the ferromagnetic-proximity induced effects, we model the entire system in the following way. Magnetic molecule is described by a single molecular level, through which the electronic transport takes place, which is exchange-coupled to magnetic core of the molecule specified by the effective spin $\mathbf{S}_{\text{MC}}$. Thus the molecule can be expressed by the Hamiltonian

$$H_{\text{SMM}} = \underbrace{\varepsilon n + U n_\uparrow n_\downarrow}_{\text{molecular level}} - J\mathbf{S}_{\text{MC}} \cdot \mathbf{s}, \tag{2}$$

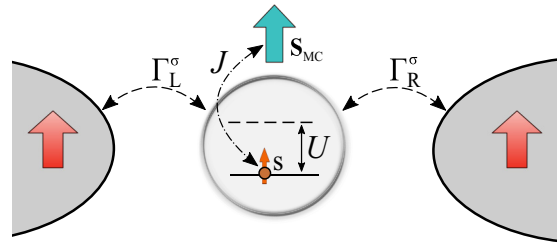

FIG. 1. Schematic of the considered system. A large-spin molecule with a molecular level is coupled to external spin-polarized leads with the spin-dependent coupling strengths $\Gamma_{\text{L}}^{\sigma}$ and $\Gamma_{\text{R}}^{\sigma}$, for the left and right lead. The molecular level is exchange-coupled to magnetic core spin of the molecule with strength J. Coulomb correlations of the molecule are denoted by U.

where the level occupation is expressed as, $n = n_\uparrow + n_\downarrow = d_\uparrow^\dagger d_\uparrow + d_\downarrow^\dagger d_\downarrow$, with $d_\sigma^\dagger(d_\sigma)$ being the fermionic creation (annihilation) operator for an electron with spin σ. The molecular level energy is denoted by ε and the Coulomb correlations are described by U. We assume ferromagnetic exchange interaction $J > 0$ between the spin of the electron on the orbital level $\mathbf{s}$ and the magnetic core spin $\mathbf{S}_{\text{MC}}$. The total spin is then expressed as $S = \mathbf{S}_{\text{MC}} + \mathbf{s}$.

The molecule is coupled to left and right spin-polarized ferromagnetic leads [61,62,75,76], see Fig. 1. Here, we exploit the correspondence between the coupling to two leads at equilibrium with the magnetic moments arranged in the parallel configuration and the coupling to a single ferromagnetic lead. The equivalence can be shown by carrying out an orthogonal transformation [33], after which the central part of the system couples exclusively to even linear combination of reservoir operators with effective coupling strength $\Gamma^\sigma = \Gamma_{\text{L}}^\sigma + \Gamma_{\text{R}}^\sigma$ and spin polarization p. Consequently, the leads can be described by an effective reservoir of noninteracting quasiparticles

$$H_{\text{Lead}} = \sum_{\mathbf{k}\sigma} \varepsilon_{\mathbf{k}\sigma} c_{\mathbf{k}\sigma}^\dagger c_{\mathbf{k}\sigma}, \tag{3}$$

where $c_{\mathbf{k}\sigma}^\dagger(c_{\mathbf{k}\sigma})$ is the creation (annihilation) operator of an electron with momentum $\mathbf{k}$, spin σ and energy $\varepsilon_{\mathbf{k}\sigma}$, which is given by appropriate linear combination of electron operators in the left and right leads. On the other hand, the spin-dependent coupling is specified by the tunneling term

$$H_{\text{Tun}} = \sum_{\mathbf{k}\sigma} V_\sigma (c_{\mathbf{k}\sigma}^\dagger d_\sigma + \text{H.c.}), \tag{4}$$

where V_σ are the effective tunnel matrix elements, assumed to be momentum independent.

The spin-dependent coupling between the molecule and the effective lead is expressed as, $\Gamma^\sigma = \pi\rho^\sigma |V_\sigma|^2$, with ρ^σ being the spin-dependent density of states of ferromagnetic electrodes. By introducing the spin polarization of the leads p, the coupling strength can be written in the following manner, $\Gamma^{\uparrow(\downarrow)} = \Gamma(1 \pm p)$, with $\Gamma^{\uparrow(\downarrow)}$ denoting the coupling to the spin-up (spin-down) electron band of the ferromagnetic reservoir and $\Gamma = (\Gamma^\uparrow + \Gamma^\downarrow)/2$.

Finally, the full Hamiltonian of the considered system reads

$$H = H_{\text{SMM}} + H_{\text{Lead}} + H_{\text{Tun}}. \tag{5}$$

B. Quench protocol and NRG implementation

The time-dependent Hamiltonian describing the dynamics after a quantum quench has the following general form

$$H(t) = \theta(-t)H_0 + \theta(t)H, \tag{6}$$

where the Hamiltonian H_0 denotes the initial Hamiltonian of the system. On the other hand, H is the Hamiltonian describing the time evolution after the sudden quench at time $t = 0$ and $\theta(t)$ is the Heaviside step function. Both Hamiltonians have a form outlined in Eq. (5) with appropriate parameters modified according to the evaluated quench. The time-dependent expectation value of a given local operator $\mathcal{O}(t)$ can be calculated from

$$O(t) \equiv \langle \mathcal{O}(t) \rangle = \mathrm{Tr}\{e^{-iHt}\rho_0 e^{iHt}\mathcal{O}\}. \tag{7}$$

Here, ρ_0 is the initial density matrix of the system described by the Hamiltonian H_0.

Let us now briefly discuss the most important aspects concerning the NRG implementation of the quench calculations [67–69]. The essential part of the NRG procedure is the logarithmic discretization of the conduction band followed by mapping of the discretized Hamiltonian to a one-dimensional tight-binding chain called the Wilson chain [68]. This step is performed for both Hamiltonians H and H_0. Subsequently, the two Hamiltonians are independently solved in an iterative fashion using the NRG procedure [69]. At each iteration, there are states that are used to construct the state-space of the next iteration and the states that are discarded. The discarded states are used to create the full many-body eigenbases [70]

$$\sum_{nse} |nse\rangle_0^D\, {}_0^D\langle nse| = \mathbb{1} \quad \text{and} \quad \sum_{nse} |nse\rangle^D\, {}^D\langle nse| = \mathbb{1}, \tag{8}$$

of both Hamiltonians, H_0 and H, respectively, and to construct the full density matrix ρ_0 at temperature $T \equiv 1/\beta$ [77]

$$\rho_0 = \sum_{nse} \frac{e^{-\beta E^D_{0ns}}}{Z} |nse\rangle_0^D\, {}_0^D\langle nse|, \tag{9}$$

where

$$Z \equiv \sum_{nse} e^{-\beta E^D_{0ns}} \tag{10}$$

is the partition function. Here, s denotes a state at Wilson site n, while e corresponds to an environmental state describing the rest of the chain.

The time-dependent expectation value $\langle \mathcal{O}(t) \rangle$ of an operator $\mathcal{O}$ can be conveniently evaluated in the frequency space and then Fourier-transformed to the time domain [78]. The frequency-dependent expectation value $\langle \mathcal{O}(\omega) \rangle$ of a local operator $\mathcal{O}$ expressed in the corresponding eigenstates of the two Hamiltonians is given by [79]

$$\langle \mathcal{O}(\omega) \rangle = \sum_{n}^{XX' \neq KK} \sum_{n'} \sum_{ss'e} {}^X\langle nse|w_{n'}\rho_{0n'}|ns'e\rangle^{X'} \times {}^{X'}\langle ns'e|\mathcal{O}|nse\rangle^X\, \delta\big(\omega + E^X_{ns} - E^{X'}_{ns'}\big). \tag{11}$$

where $X = K(X = D)$ denotes a kept (discarded) state. Here, $\rho_{0n'}$ is the contribution of the density matrix coming from iteration n' and $w_{n'}$ is the corresponding weight.

We also use NRG to determine the linear-response conductance between the two ferromagnetic leads from the following formula [80]:

$$G = \frac{e^2}{h}\pi\Gamma \int d\omega \left(-\frac{\partial f}{\partial \omega}\right)[(1+p)A_\uparrow(\omega) + (1-p)A_\downarrow(\omega)], \tag{12}$$

where $A_\sigma(\omega)$ is the molecular level spectral function, defined as $A_\sigma(\omega) = -(1/\pi)\mathrm{Im}\langle\langle d_\sigma | d^\dagger_\sigma \rangle\rangle^R_\omega$, with $\langle\langle d_\sigma | d^\dagger_\sigma \rangle\rangle^R_\omega$ being the Fourier transform of the retarded Green's function $\langle\langle d_\sigma | d^\dagger_\sigma \rangle\rangle^R_t = -i\theta(t)\langle\{d_\sigma(t), d^\dagger_\sigma(0)\}\rangle$.

For the NRG calculations we used the discretization parameter $2 \leqslant \Lambda \leqslant 3$, set the length of the Wilson chain to be $N = 80$ and kept at least $N_K = 4000$ energetically lowest-lying states at each iteration. In order to suppress the band discretization effects, we also used the Oliveira's z averaging [81] by performing calculations for $N_z = 4$ different discretizations. More details and technicalities concerning the implementation of calculations can be found in Ref. [79].

III. RESULTS AND DISCUSSION

A. Static properties of the molecule

In order to obtain a better understanding of the magnetic correlations present in the considered system, let us first examine the static properties. As the main focus is put on the quadrupolar field, we tune the system to the particle-hole symmetry point by setting the energy of the orbital level to $\varepsilon = -U/2$. As a result, the dipolar field vanishes [61] and only quadrupolar term is present in the system [second term of Eq. (1)]. This approach allows us to precisely describe the generated uniaxial anisotropy, quantified by the amplitude D, see Eq. (1).

In Fig. 2(a), we present the spin-quadrupole moment $\langle \mathcal{Q}_{zz} \rangle$ and expectation values of the corresponding spin operators, $\langle S^2 \rangle$ and $\langle S_z^2 \rangle$, as the coupling strength Γ is varied. The general behavior of spin-quadrupole moment (dark-blue line) is that in the weak-coupling regime ($\Gamma/U \lesssim 10^{-1}$), it acquires the value $\langle \mathcal{Q}_{zz} \rangle = S(2S-1)/3 = 1$, while in the strong-coupling regime ($\Gamma/U \gtrsim 10^{-1}$), this value is strongly reduced to $\langle \mathcal{Q}_{zz} \rangle = \mathbf{S}_{\mathrm{MC}}(2\mathbf{S}_{\mathrm{MC}} - 1)/3 = 1/3$. The suppression of the moment in the strong-coupling regime is due to the presence of the Kondo correlations. The Kondo effect is exposed in the conductance dependence (yellow line), as it saturates to unitary value $G/G_0 = 1$ in the strong-coupling regime. In consequence, the spin of the molecular level is screened, and the total spin of the molecule is reduced from $S = 3/2$ to $S = \mathbf{S}_{\mathrm{MC}} = 1$, leading eventually to $\langle \mathcal{Q}_{zz} \rangle = 1/3$. To clearly show how the expectation values of spin operators influence the value of the spin-quadrupole moment, we also plot $\langle S^2 \rangle$ and $\langle S_z^2 \rangle$ as a function of the coupling strength. It is noteworthy that both quantities in the Kondo regime do not achieve the value, that would be expected when electron on the orbital level was fully screened by the Kondo correlations. The expected values only approach this limit, i.e., $\langle S^2 \rangle \to 2$, $\langle S_z^2 \rangle \to 1$, however, the resulting value of the spin-quadrupole moment is indeed $\langle \mathcal{Q}_{zz} \rangle = 1/3$.

In Fig. 2(b), we present the spin-quadrupole moment $\langle \mathcal{Q}_{zz} \rangle$ (solid lines) and the linear-response conductance G (dashed lines) as a function of Γ for different values of the exchange

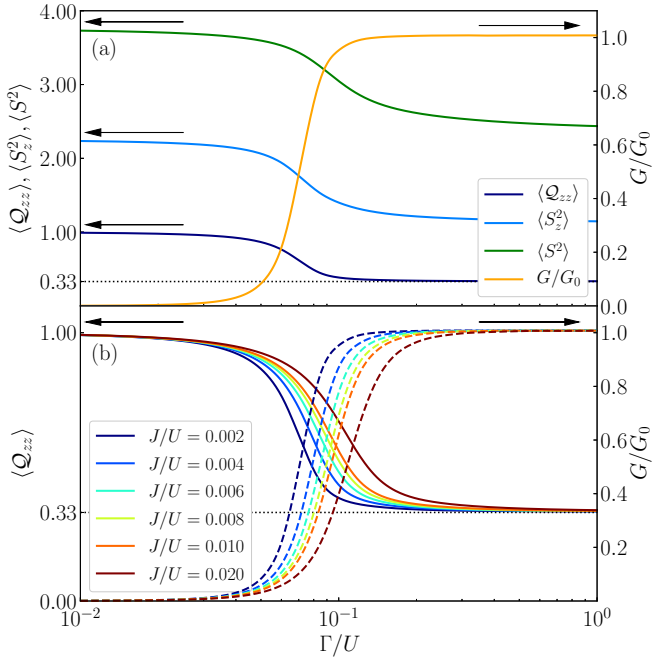

FIG. 2. (a) The spin-quadrupole moment $\langle \mathcal{Q}_{zz} \rangle$ expectation values of the corresponding spin operators, $\langle S^2 \rangle$ and $\langle S_z^2 \rangle$, and normalized linear-response conductance G, with $G_0 = 2e^2/h$, for $S = 3/2$ spin molecule as a function of the coupling strength Γ. The parameters are $U = 1/2$, $\varepsilon/U = -1/2$, $J/U = 2 \times 10^{-3}$, in units of band halfwidth $W \equiv 1$, $p = 0.5$, and temperature $T/U \sim 10^{-18}$. (b) The spin-quadrupole moment $\langle \mathcal{Q}_{zz} \rangle$ (solid lines) and normalized linear-response conductance G (dashed lines) plotted vs Γ for different values of exchange coupling J.

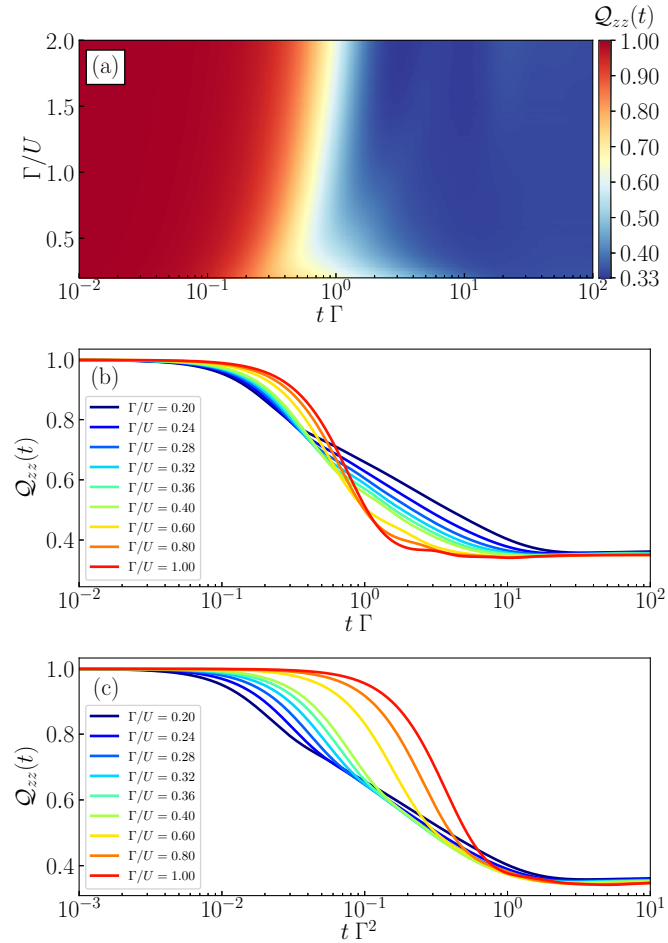

FIG. 3. The time dependence of the spin-quadrupole moment $\mathcal{Q}_{zz}(t)$ after quench in the coupling strength from $\Gamma_0/U = 0.002$ to different values of the final coupling strength. (a) presents the density plot of $\mathcal{Q}_{zz}(t)$, while (b) and (c) show $\mathcal{Q}_{zz}(t)$ as a function of $t\,\Gamma$ and $t\,\Gamma^2$, respectively. The other parameters are the same as in Fig. 2(a).

coupling J. As evident, when the magnitude of J is varied, the spin-quadrupole moment values in the weak and strong-coupling regimes are conserved, however, the increase of the exchange coupling extends the transitional range of coupling strength where the crossover between the weak and Kondo regimes develops. Although the considered model is an effective one, we expect that in the case of molecules with strong exchange couplings between localized spins and those of itinerant electrons, the quench in the coupling strength needs to be superior than in the case of systems with small magnitudes of the exchange couplings. The role of magnitude of J on the dynamics of the spin-quadrupole moment is discussed in more detail in Sec. III C.

B. Dynamics of quadrupole moment

The important alteration in the SMM's magnetic properties is when the coupling strength Γ is switched from the weak-coupling regime, where the spin-quadrupole moment is saturated acquiring $\langle \mathcal{Q}_{zz} \rangle = S(2S-1)/3 = 1$, to the strong-coupling regime. In the latter case, the Kondo correlations are present and the moment is reduced to $\langle \mathcal{Q}_{zz} \rangle = \mathbf{S}_{\mathrm{MC}}(2\mathbf{S}_{\mathrm{MC}} - 1)/3 = 1/3$.

In order to study the dynamics of this effect, we perform a quantum quench of the initial Hamiltonian H_0 in the coupling strength from $\Gamma_0/U = 0.002$ to various final values of Γ/U in the range of strong-coupling where the Kondo effect is well-established. In Fig. 3(a), we display the resulting time dependence of the spin-quadrupole moment $\mathcal{Q}_{zz}(t)$. First of all, independently of Γ, both initial $\mathcal{Q}_{zz}(t=0)$ and final $\mathcal{Q}_{zz}(t \to \infty)$ are in agreement with thermal expectation values. As can be seen, the long-term value is also independent of the coupling strength Γ as long as the final coupling strength is within the strong-coupling regime, here $\Gamma/U \gtrsim 0.1$, indicated by the unitary conductance, see Fig. 2. However, the value of Γ clearly influences the dynamics of the transition. In the short-time limit, the initial value of $\langle \mathcal{Q}_{zz} \rangle = 1$ holds for at least time $t\,\Gamma \approx 10^{-1}$. The reduction of quadrupole moment takes place for times $t\,\Gamma \gtrsim 10^{-1}$, and the dependence of this process is influenced by the final coupling strength. In the range of $0.4 \gtrsim \Gamma/U \gtrsim 0.2$, the drop of $\mathcal{Q}_{zz}(t)$ is observable as early as $t\,\Gamma \approx 2 \times 10^{-1}$ and at middle rate approaches the long-time limit for times $t\,\Gamma \gtrsim 10^{1}$. However, when the quench is evaluated for higher values of the final coupling strength, the time dependence is more rapid. On one side, $\mathcal{Q}_{zz}(t)$ starts to drop at later times, $t\,\Gamma \approx 5 \times 10^{1}$ for $\Gamma/U = 2$, but on the other side, it achieves long-time limit significantly faster, i.e., $\mathcal{Q}_{zz}(t = 2/\Gamma) \approx \mathcal{Q}_{zz}(t \to \infty)$ also for $\Gamma/U = 2$. Therefore,

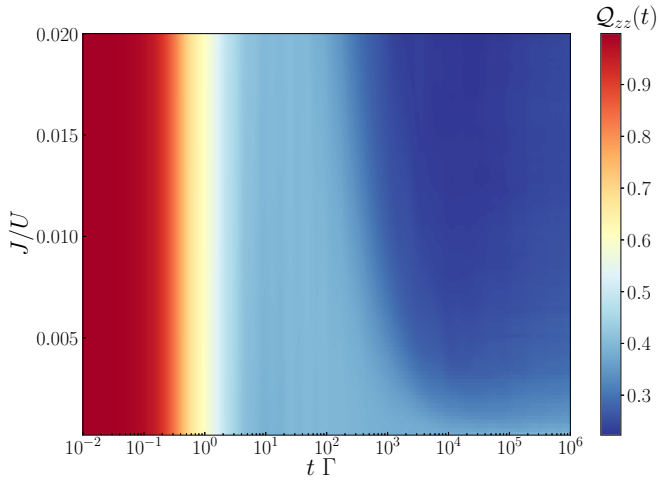

FIG. 4. The spin-quadrupole moment $\mathcal{Q}_{zz}(t)$ after the quench from the weak to the strong-coupling regime ($\Gamma_0/U = 0.002$ and $\Gamma/U = 0.4$) as a function of time and exchange interaction J/U. The other parameters are the same as in Fig. 2.

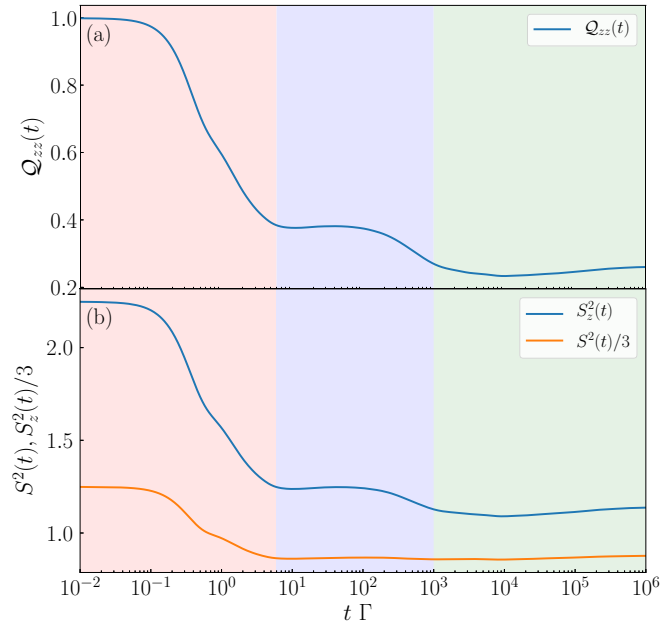

FIG. 5. The time dependence of the spin-quadrupole moment $\mathcal{Q}_{zz}(t)$ and the expectation values of $S_z^2(t)$ and $S^2(t)/3$ after quench in the coupling strength from $\Gamma_0/U = 0.002$ to $\Gamma/U = 0.4$. The exchange coupling is set to $J/U = 0.01$. The other parameters are the same as in Fig. 2.

by tuning the value of the final coupling strength Γ, the timescale of the considered transition can be varied by an order of magnitude.

To clearly display the above behavior, in Fig. 3(b), we show the time evolution of quadrupolar moment for different values of Γ chosen from the range, where the dynamics is most interesting. Finally, in Fig. 3(c), we show the same results in the form of several curves on a rescaled time axis in order to clearly indicate that the relaxation is universally governed by $t \propto 1/\Gamma^2$. The long-time limit is achieved at times $t \approx 2/\Gamma^2$, when one can see that all the curves converge.

C. Role of molecule's exchange coupling

An important impact on the magnetic and transport properties of SMM systems has the magnitude of exchange coupling J between the effective magnetic core spin $\mathbf{S}_{\mathrm{MC}}$ and the spin $\mathbf{s}$ of electrons occupying the orbital level. In Fig. 4, we show the time-dependent spin-quadrupole moment, considering similar quench as in previous section, with $\Gamma_0/U = 0.002$ and $\Gamma/U = 0.4$, as a function of exchange coupling J.

It can be clearly seen that the magnitude of J does not have a substantial influence on the short time evolution of spin-quadrupole moment for elapsed time up to $t\,\Gamma \approx 10^2$. For $J/U \lesssim 0.002$, the long-time limit $\langle \mathcal{Q}_{zz} \rangle = 1/3$ is achieved already around $t\,\Gamma \approx 10^1$ and there is no further dynamics as the time elapses. However, when the exchange coupling is increased above $J/U \approx 0.002$, further decrease of spin-quadrupole moment takes place at long times, i.e., for $t\,\Gamma \gtrsim 10^2$. The observed reduction is down to values well below $\langle \mathcal{Q}_{zz} \rangle = 1/3$, i.e., $\mathcal{Q}_{zz}(t \to \infty) \lesssim 0.3$, and the dynamics of this process is strongly dependent on the magnitude of J. When the time dependence for larger values of J is evaluated, the new long-time limit is achieved at earlier times, while the value of spin-quadrupole moment is accordingly further suppressed.

In order to better understand the effect of exchange coupling on the spin-quadrupole moment dynamics, we examine the time dependence of two spin operators, $S_z^2(t)$ and $S^2(t)/3$, which are the constituent components of the operator $\mathcal{Q}_{zz}(t)$. The corresponding plots are shown in Fig. 5. The results were obtained for exchange coupling set to $J/U = 0.01$, where the time dependence reveals two stages of magnetic moment reduction. In Fig. 5(a), we display the time-dependent spin-quadrupole moment after the quench in the coupling strength, while in Fig. 5(b), we present the time-dependent expectation values of spin operators $S_z^2(t)$ and $S^2(t)/3$.

To highlight the most important stages of the dynamics, we marked three time ranges with respective pale colors. The red background contains short-time dynamics, when a rapid suppression of all expectation values takes places in a similar manner like in the case of weaker J coupling. This dynamics is associated with the change of the ground state and the reduction of the total spin S from $S = 3/2$ to $S = 1$ due to the Kondo screening of the orbital spin. This stage of time evolution ends up at times around $t\,\Gamma \approx 10^1$. Consequently, the next section is marked with purple background and contains the further dynamics associated with influence of the exchange interaction J. For times $t\,\Gamma \gtrsim 10^1$, the time dependence of the spin operators clearly shows that the total spin of the system S remains intact and has already achieved the long-time limit. Further ongoing dynamics takes place exclusively for $S_z^2(t)$ in the form of second stage of slow suppression of the total spin-quadrupole moment to $\mathcal{Q}_{zz}(t) \lesssim 1/3$. The total time of this stage evolution greatly depends on the strength of J, as shown in Fig. 4, i.e., the system faster reaches equilibrium for higher values of the exchange coupling J.

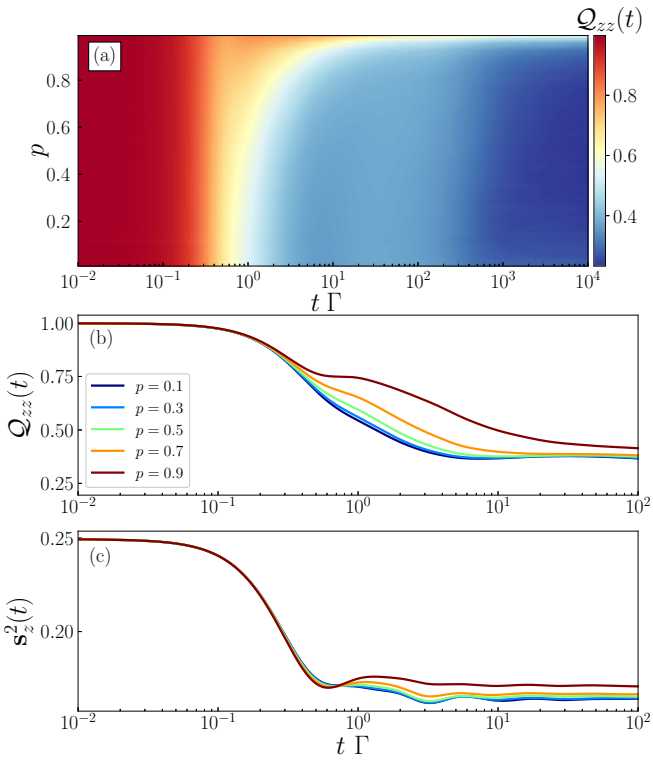

FIG. 6. (a) The spin-quadrupole moment $\mathcal{Q}_{zz}(t)$ after a quench from the weak to the strong-coupling regime as a function of time and spin polarization p. (b) The spin-quadrupole moment $\mathcal{Q}_{zz}(t)$ and (c) square of the molecular level's magnetization $\mathbf{s}_z^2(t)$ after the quench as a function of $t\,\Gamma$ shown for several values of p. The other parameters are the same as in Fig. 5.

D. Influence of lead spin polarization

The ferromagnetism of the leads is of great importance for the considered molecular system. In general, when a finite spin polarization of electrodes is assumed ($p > 0$) and their magnetic moments are aligned, the effective dipolar and quadrupolar exchange fields are generated [53,62]. The strengths of these fields and their occurrence strongly depend on the degree of spin polarization p. In our analysis, we focus on the quadrupolar term by tuning the molecular level to the particle-hole symmetry point $\varepsilon = -U/2$. In such a configuration, the charge fluctuations for both spin directions are equal and independently of the magnitude of p the dipolar field is canceled. Moreover, it was shown that for large-spin molecules, a very small spin polarization ($p = 0.01$) of the leads can give rise to $\langle \mathcal{Q}_{zz} \rangle = S(2S-1)/3 = 1$. In equilibrium, a similar dependence to that shown in Fig. 2 is predicted for wide range of p, with finite temperature suppressing the spin-quadrupole moment in the regime of very weak-coupling strengths [65]. Therefore, let us now discuss the influence of leads spin polarization p on the dynamics of the spin-quadrupole moment after the quench from the weak to the strong-coupling regime ($\Gamma_0/U = 0.002$ and $\Gamma/U = 0.4$). The results presenting $\mathcal{Q}_{zz}(t)$ for a wide range of spin polarizations p are shown in Fig. 6(a).

In the range of small and moderate spin polarizations ($p \lesssim 0.4$), the time evolution of spin quadrupole moment has both qualitatively and quantitatively similar dependence, with two stages of $\mathcal{Q}_{zz}(t) = 1$ reduction present, as discussed in previous section for the case of significant exchange coupling $J/U = 0.01$. However, when the spin polarization is increased further ($p \gtrsim 0.4$), a new step emerges right before the time $t\,\Gamma \approx 1$, when $\mathcal{Q}_{zz}(t) \approx 3/4$. This step is elongated as p is increased, reaching times up to $t\,\Gamma \approx 10^1$ for $p = 0.9$ and eventually not fully relaxing to $\mathcal{Q}_{zz}(t) = 1/3$, when $p \to 1$. This behavior might seem to be counter-intuitive, as one could expect that with increased spin polarization of the leads, the dynamics of the quench should be faster along with rapid suppression of the spin-quadrupole moment. Here, we predict quite opposite dependence, as the dynamics is faster and more straightforward when the spin polarization of the leads has low-to-moderate values.

The mechanism responsible for the emergence of an additional step in $\mathcal{Q}_{zz}(t)$ in the case of highly spin-polarized electrodes is closely related to an enhanced difference between spin-dependent couplings $\Gamma^{\uparrow} = \Gamma(1+p)$ and $\Gamma^{\downarrow} = \Gamma(1-p)$ whilst p is increased. The bottleneck of the associated dynamics is governed by the coupling to the minority band, which in result slows down the dynamics of the spin-quadrupole moment. To clearly analyze the discussed effect, we show the spin-quadrupole moment $\mathcal{Q}_{zz}(t)$ in Fig. 6(b) and the square of molecular-level magnetization $\mathbf{s}_z^2(t)$ in Fig. 6(c) as a function of $t\,\Gamma$. Here, we recall that molecular-level magnetization is defined as $\mathbf{s}_z(t) = (n_{\uparrow}(t) - n_{\downarrow}(t))/2$. The discussed dynamics revealed for highly spin-polarized lead takes place at times $t\,\Gamma \lesssim 1$. The effect is evident for $p = 0.9$, where the dependence of $\mathcal{Q}_{zz}(t)$ exposes a short plateau with $\mathcal{Q}_{zz}(t) \approx 3/4$. The time dependence of the local operator $\mathbf{s}_z^2(t)$ plays an important role here. As can be seen in the figure, $\mathbf{s}_z^2(t)$ is a monotonically decreasing function of time for $p \lesssim 0.7$ in this time regime. Interestingly, further enhancement of spin polarization generates a subtle oscillation in the time dependence of $\mathbf{s}_z^2(t)$. In that time range, $\Gamma^{\uparrow} = \Gamma(1+p)$ is responsible for a rapid drop of $\mathbf{s}_z^2(t)$ due to decrease of the spin-up component. However, the time evolution is not balanced by the spin-down component due to a significantly slower dynamics governed by $\Gamma^{\downarrow} = \Gamma(1-p)$. As a result, the molecular level has a minimum in $\mathbf{s}_z^2(t)$, which is below the long-time limit thermal value, at time $t\,\Gamma \approx 6 \times 10^{-1}$, see Fig. 6(c). Subsequently, a small increase takes places leading to eventual relaxation. This nonmonotonic dependence of $\mathbf{s}_z^2(t)$ is observed as a result of the interplay between the spin-dependent couplings and, in consequence, temporarily pauses the reduction of $\mathcal{Q}_{zz}(t)$. A similar dynamical behavior was predicted for the magnetization of a single quantum dot system coupled to ferromagnetic lead [79].

E. Influence of magnitude of molecular spin

In order to generalize our analysis for magnetic molecules of arbitrarily given total spin S, we examine the results of tNRG calculations for models with different values of magnetic core spin $\mathbf{S}_{\mathrm{MC}}$. First of all, we would like to note that in equilibrium, qualitatively a very similar dependence of $\langle \mathcal{Q}_{zz} \rangle$ on the coupling strength Γ is expected independently of the value of $\mathbf{S}_{\mathrm{MC}}$, see Fig. 7(a). As the spin of magnetic core is increased, the maximal value of the spin-quadrupole moment

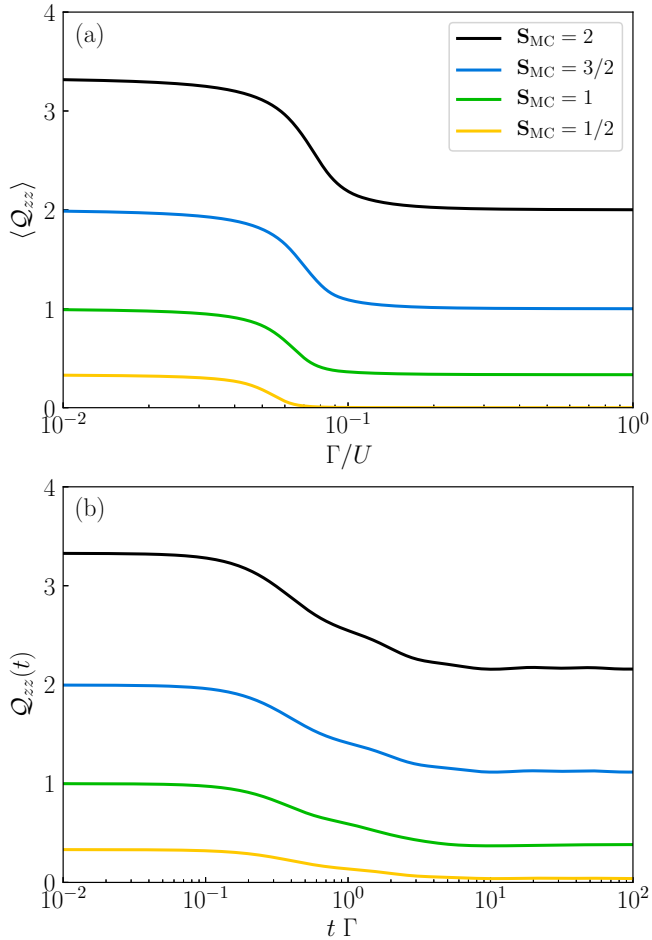

FIG. 7. (a) The static value of spin-quadrupole moment $\mathcal{Q}_{zz}$ for different values of $\mathbf{S}_{\mathrm{MC}}$ as a function of coupling Γ and (b) $\mathcal{Q}_{zz}(t)$ for several values of $\mathbf{S}_{\mathrm{MC}}$ as a function of time elapsed after the quench in the coupling Γ. The parameters are the same as in Fig. 2(a).

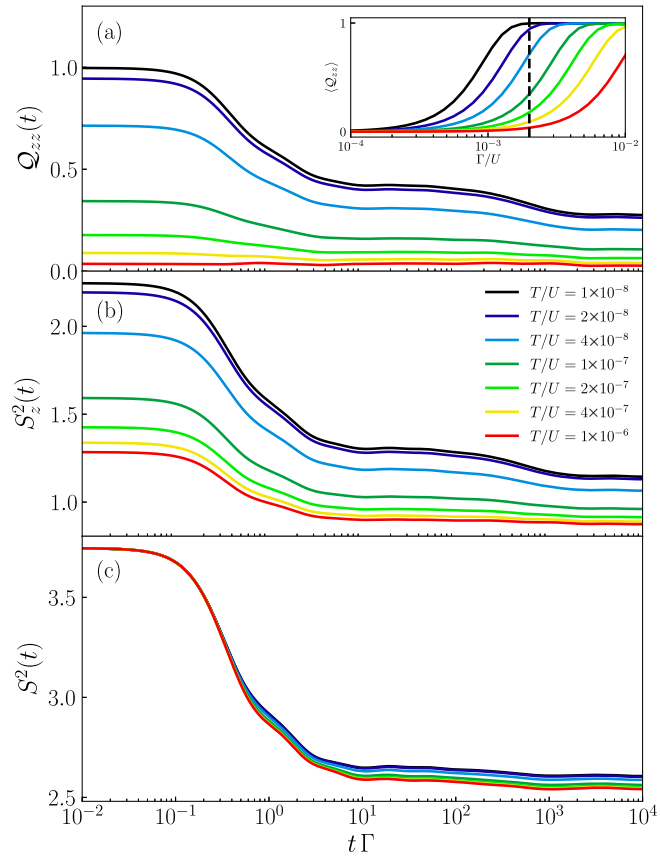

FIG. 8. (a) The spin-quadrupole moment $\mathcal{Q}_{zz}(t)$, (b) $S_z^2(t)$ and (c) $S^2(t)$ for several values of temperature T plotted as a function of time elapsed after the quench in Γ. The inset in (a) shows the influence of temperature on the static value of the spin-quadrupole moment in the weak-coupling regime. Dashed vertical line indicates the initial value of the coupling strength. The parameters are the same as in Fig. 5.

in the weak-coupling regime is increasing accordingly with $\langle \mathcal{Q}_{zz} \rangle = S_z^2 - S(S+1)/3$. Furthermore, the transition range of coupling strengths preceding the strong-coupling regime is similar for all cases, i.e., $5 \times 10^{-2} \lesssim \Gamma/U \lesssim 2 \times 10^{-1}$. Eventually, the important change influenced by the total spin of the molecule is in the value, by which the spin-quadrupole moment is reduced, when the coupling regime is switched from the weak to the strong one. This difference is enhanced, when the total spin number is increased.

The time-dependent spin-quadrupole moment after the quench as a function of time for several values of S_{MC} is shown in Fig. 7(b). Here, one can see that the dynamics is still governed by the strength of coupling to electrodes, as the reduction of spin-quadrupolar moment starts and achieves long-time limit at similar moments on the time axis rescaled with Γ. For all considered values of $\mathbf{S}_{\mathrm{MC}}$, time-evolutions behave in a similar fashion with the main distinction of initial and final values of $\langle \mathcal{Q}_{zz} \rangle$ and the rate of reduction. Similar effects and dependencies due to the exchange interaction or spin polarization of the leads as discussed in previous sections are predicted also for molecules with even higher total spin number (not shown here). Therefore, our dynamical studies presented in this work have a general character and are valid for broad range of SMM systems, in which the quadrupolar exchange field emerges from ferromagnetic proximity effect.

F. Finite temperature effects

Lastly, we examine the influence of finite temperature T on the spin-quadrupole moment and its time evolution following the quench in the coupling. In Fig. 8, we show the time-dependent expectation value of the spin-quadrupole moment as well as the corresponding spin operators for several values of temperatures.

For the regime of very low temperatures, $T/U \lesssim 10^{-8}$, both the initial and final values, as well as the quench dynamics of the spin-quadrupole moment remain similar to the case of zero temperature. Further increase of temperature, however, has a significant impact on the system's behavior. First of all, the initial value of the spin quadrupole moment in the weak-coupling regime is significantly suppressed as the temperature is increased. The inset in Fig. 8(a) shows how the increase of temperature reduces the static spin-quadrupole moment in the weak-coupling regime. The vertical dashed line represents the initial coupling strength $\Gamma_0/U = 0.002$ that we have used in the evaluation of the quench dynamics. From the

above considerations, it is evident that the fine tuning of the coupling strength for the initial state is critical, in particular when the suppression of the maximal value of the moment is expected. Furthermore, the long-time limit value of the time-dependent spin-quadrupole moment is also reduced by the temperature, however, not as strongly as the initial value. In consequence, as the temperature is increased, the whole transient dynamics is exposing more moderate dependence, with almost completely flat one for temperatures $T/U \gtrsim 10^{-6}$. It is also important to note, that all the characteristic timescales discussed in earlier analysis for $T = 0$ are conserved for the finite temperatures, where a considerable suppression of spin-quadrupole moment is predicted. In particular, the rapid reduction associated with the change of the ground state that dominates the dynamics for times $t\,\Gamma \lesssim 10^{1}$ and further slower dynamics influenced by the exchange coupling taking place for times up to $t\,\Gamma \approx 10^{3}$ are all still noticeable for temperatures up to $T/U \approx 10^{-7}$.

The inspection of the spin operators $S_z^2(t)$ and $S^2(t)$, see Figs. 8(b) and 8(c), brings the conclusion that the temperature influences spin-quadrupole moment only by reduction of the z-th component of the SMM's spin. Meanwhile the square value of the total spin remains unaffected, as it corresponds to the change of the molecule's ground state. This fact clearly indicates the reduction of the molecule's magnetic anisotropy due to thermal fluctuations.

IV. CONCLUSIONS

We have analyzed the quench dynamics of large-spin magnetic molecules attached to spin-polarized ferromagnetic leads. The study was performed by using the time-dependent numerical renormalization group method. We focused on the dynamics of the spin-quadrupole moment and a quench associated with switching the system from the weak-coupling regime to the strong-coupling one, in which the Kondo correlations are present and the screening of the molecular level spin develops.

In general, we have shown that the time necessary to achieve the new thermal value in the strong-coupling regime is inversely proportional to squared coupling strength, i.e., $t \propto 1/\Gamma^2$. Furthermore, we examined the role of ferromagnetic exchange coupling J and showed that when the magnitude of this interaction is considerable, additional step in the time dependence emerges, corresponding to slower dynamics mediated by J, which is an interesting case of interplay between the Kondo correlations and ferromagnetism exposed in our dynamical studies. The influence of electrodes spin polarization was also discussed, strongly indicating that the quench dynamics is faster and more straightforward for low-to-average values. We also generalized our studies to systems with higher total spin numbers to show that observations and conclusions are valid for a wide class of SMM systems with arbitrary total spin number.

Finally, we studied the influence of finite temperature on the spin-quadrupole moment. A strong suppression of the time-dependent value is predicted in certain range of temperatures, due to reduction of the molecululer anisotropy. The important role of the coupling strength fine tuning is also indicated, which may have relevance for the experiments.

ACKNOWLEDGMENTS

This work was supported by the Polish National Science Centre from funds awarded through the decision No. 2017/27/B/ST3/00621. The computing time at the Poznań Supercomputing and Networking Center is acknowledged.

[1] R. Boča, *Theoretical Foundations of Molecular Magnetism* (Elsevier, New York, 1999).

[2] J. Tejada, E. M. Chudnovsky, E. del Barco, J. M. Hernandez, and T. P. Spiller, Magnetic qubits as hardware for quantum computers, Nanotechnology **12**, 181 (2001).

[3] D. Gatteschi, R. Sessoli, and J. Villain, *Molecular Nanomagnets* (Oxford University Press, Oxford, 2006).

[4] L. Bogani and W. Wernsdorfer, Molecular spintronics using single-molecule magnets, Nat. Mater. **7**, 179 (2008).

[5] J. Lehmann, A. Gaita-Ariño, E. Coronado, and D. Loss, Quantum computing with molecular spin systems, J. Mater. Chem. **19**, 1672 (2009).

[6] M. Mannini, F. Pineider, P. Sainctavit, C. Danieli, E. Otero, C. Sciancalepore, A. M. Talarico, M.-A. Arrio, A. Cornia, D. Gatteschi, and R. Sessoli, Magnetic memory of a single-molecule quantum magnet wired to a gold surface, Nat. Mater. **8**, 194 (2009).

[7] R. Vincent, S. Klyatskaya, M. Ruben, W. Wernsdorfer, and F. Balestro, Electronic read-out of a single nuclear spin using a molecular spin transistor, Nature (London) **488**, 357 (2012).

[8] P. Jacobson, T. Herden, M. Muenks, G. Laskin, O. Brovko, V. Stepanyuk, M. Ternes, and K. Kern, Quantum engineering of spin and anisotropy in magnetic molecular junctions, Nat. Commun. **6**, 8536 (2015).

[9] R. Sessoli, Magnetic molecules back in the race, Nature (London) **548**, 400 (2017).

[10] K. Najafi, A. L. Wysocki, K. Park, S. E. Economou, and E. Barnes, Toward long-range entanglement between electrically driven single-molecule magnets, J. Phys. Chem. Lett. **10**, 7347 (2019).

[11] P. Gambardella, S. Rusponi, M. Veronese, S. S. Dhesi, C. Grazioli, A. Dallmeyer, I. Cabria, R. Zeller, P. H. Dederichs, K. Kern, C. Carbone, and H. Brune, Giant magnetic anisotropy of single cobalt atoms and nanoparticles, Science **300**, 1130 (2003).

[12] C. F. Hirjibehedin, C.-Y. Lin, A. F. Otte, M. Ternes, C. P. Lutz, B. A. Jones, and A. J. Heinrich, Large magnetic anisotropy of a single atomic spin embedded in a surface molecular network, Science **317**, 1199 (2007).

[13] P. Gambardella, S. Stepanow, A. Dmitriev, J. Honolka, F. M. F. de Groot, M. Lingenfelder, S. S. Gupta, D. D. Sarma, P. Bencok, S. Stanescu, S. Clair, S. Pons, N. Lin, A. P. Seitsonen, H. Brune, J. V. Barth, and K. Kern, Supramolecular control of the magnetic anisotropy in two-dimensional

high-spin Fe arrays at a metal interface, Nat. Mater. **8**, 189 (2009).

[14] L. Xu, Z. Zangeneh, R. Yadav, S. Avdoshenko, J. van den Brink, A. Jesche, and L. Hozoi, Spin-reversal energy barriers of 305 K for $Fe^{2+}d^6$ ions with linear ligand coordination, Nanoscale **9**, 10596 (2017).

[15] A. L. Wysocki and K. Park, Nature of hyperfine interactions in $TbPc_2$ single-molecule magnets: Multiconfigurational *ab initio* study, Inorg. Chem. **59**, 2771 (2020).

[16] E. M. Chudnovsky and J. Tejada, *Macroscopic Quantum Tunneling of the Magnetic Moment* (Cambridge University Press, Cambridge, 1998).

[17] E. K. Brechin, C. Boskovic, W. Wernsdorfer, J. Yoo, A. Yamaguchi, E. C. Sañudo, T. R. Concolino, A. L. Rheingold, H. Ishimoto, D. N. Hendrickson, and G. Christou, Quantum tunneling of magnetization in a new $[Mn_{18}]^{2+}$ single-molecule magnet with $S = 13$, J. Am. Chem. Soc. **124**, 9710 (2002).

[18] M. Misiorny and J. Barnaś, Quantum tunneling of magnetization in single molecular magnets coupled to ferromagnetic reservoirs, EPL **78**, 27003 (2007).

[19] M. Mannini, F. Pineider, C. Danieli, F. Totti, L. Sorace, Ph. Sainctavit, M.-A. Arrio, E. Otero, L. Joly, J. C. Cezar, A. Cornia, and R. Sessoli, Quantum tunneling of the magnetization in a monolayer of oriented single-molecule magnets, Nature (London) **468**, 417 (2010).

[20] G.-H. Kim and T.-S. Kim, Electronic Transport in Single-Molecule Magnets on Metallic Surfaces, Phys. Rev. Lett. **92**, 137203 (2004).

[21] C. Timm and F. Elste, Spin amplification, reading, and writing in transport through anisotropic magnetic molecules, Phys. Rev. B **73**, 235304 (2006).

[22] M. Misiorny, I. Weymann, and J. Barnaś, Spin effects in transport through single-molecule magnets in the sequential and cotunneling regimes, Phys. Rev. B **79**, 224420 (2009).

[23] M. Misiorny, I. Weymann, and J. Barnaś, Spin diode behavior in transport through single-molecule magnets, EPL **89**, 18003 (2010).

[24] M. Misiorny, I. Weymann, and J. Barnaś, Temperature dependence of electronic transport through molecular magnets in the Kondo regime, Phys. Rev. B **86**, 035417 (2012).

[25] M. Misiorny, E. Burzurí, R. Gaudenzi, K. Park, M. Leijnse, M. R. Wegewijs, J. Paaske, A. Cornia, and H. S. J. van der Zant, Probing transverse magnetic anisotropy by electronic transport through a single-molecule magnet, Phys. Rev. B **91**, 035442 (2015).

[26] A. Płomińska and I. Weymann, Pauli spin blockade in double molecular magnets, Phys. Rev. B **94**, 035422 (2016).

[27] A. Płomińska, M. Misiorny, and I. Weymann, Manipulating spins of magnetic molecules: Hysteretic behavior with respect to bias voltage, EPL **121**, 38006 (2018).

[28] F. Pawlicki and I. Weymann, Andreev transport through single-molecule magnets, Phys. Rev. B **98**, 085411 (2018).

[29] A. Chiesa, E. Macaluso, P. Santini, S. Carretta, and E. Pavarini, First-principles many-body models for electron transport through molecular nanomagnets, Phys. Rev. B **99**, 235145 (2019).

[30] Silvia Giménez-Santamarina, Salvador Cardona-Serra, and Alejandro Gaita-Ariño, Theoretical insights on the importance of anchoring vs molecular geometry in magnetic molecules acting as junctions, J. Magn. Magn. Mater. **485**, 212 (2019).

[31] J. de Bruijckere, P. Gehring, M. Palacios-Corella, M. Clemente-León, E. Coronado, J. Paaske, P. Hedegård, and H. S. J. van der Zant, Ground-State Spin Blockade in a Single-Molecule Junction, Phys. Rev. Lett. **122**, 197701 (2019).

[32] J. Kondo, Resistance minimum in dilute magnetic alloys, Prog. of Theor. Phys. **32**, 37 (1964).

[33] L. I. Glazman and M. E. Raikh, Resonant Kondo transparency of a barrier with quasilocal impurity states, Pis'ma Zh. Eksp. Teor. Fiz. **47**, 378 (1988) [JETP Lett. **47**, 452 (1988)].

[34] A. C. Hewson, *The Kondo Problem to Heavy Fermions* (Cambridge University Press, Cambridge, 1997).

[35] D. Goldhaber-Gordon, Hadas Shtrikman, D. Mahalu, David Abusch-Magder, U. Meirav, and M. A. Kastner, Kondo effect in a single-electron transistor, Nature (London) **391**, 156 (1998).

[36] Sara M. Cronenwett, Tjerk H. Oosterkamp, and Leo P. Kouwenhoven, A tunable Kondo effect in quantum dots, Science **281**, 540 (1998).

[37] V. Madhavan, W. Chen, T. Jamneala, M. F. Crommie, and N. S. Wingreen, Tunneling into a single magnetic atom: Spectroscopic evidence of the Kondo resonance, Science **280**, 567 (1998).

[38] C. Romeike, M. R. Wegewijs, and H. Schoeller, Spin Quantum Tunneling in Single Molecular Magnets: Fingerprints in Transport Spectroscopy of Current and Noise, Phys. Rev. Lett. **96**, 196805 (2006).

[39] Alexander F. Otte, Markus Ternes, Kirsten von Bergmann, Sebastian Loth, Harald Brune, Christopher P. Lutz, Cyrus F. Hirjibehedin, and Andreas J. Heinrich, The role of magnetic anisotropy in the Kondo effect, Nat. Phys. **4**, 847 (2008).

[40] J. J. Parks, A. R. Champagne, T. A. Costi, W. W. Shum, A. N. Pasupathy, E. Neuscamman, S. Flores-Torres, P. S. Cornaglia, A. A. Aligia, C. A. Balseiro, G. K.-L. Chan, H. D. Abruña, and D. C. Ralph, Mechanical control of spin states in spin-1 molecules and the underscreened Kondo effect, Science **328**, 1370 (2010).

[41] M. Misiorny, I. Weymann, and J. Barnaś, Interplay of the Kondo Effect and Spin-Polarized Transport in Magnetic Molecules, Adatoms, and Quantum Dots, Phys. Rev. Lett. **106**, 126602 (2011).

[42] M. Misiorny, I. Weymann, and J. Barnaś, Underscreened Kondo effect in $S = 1$ magnetic quantum dots: Exchange, anisotropy, and temperature effects, Phys. Rev. B **86**, 245415 (2012).

[43] P. Zalom, J. de Bruijckere, R. Gaudenzi, H. S. J. van der Zant, T. Novotný, and R. Korytár, Magnetically tuned Kondo effect in a molecular double quantum dot: Role of the anisotropic exchange, J. Phys. Chem. C **123**, 11917 (2019).

[44] M. Misiorny and J. Barnaś, Magnetic switching of a single molecular magnet due to spin-polarized current, Phys. Rev. B **75**, 134425 (2007).

[45] G. González and M. N. Leuenberger, Berry-Phase Blockade in Single-Molecule Magnets, Phys. Rev. Lett. **98**, 256804 (2007).

[46] M. Misiorny and J. Barnaś, Effects of intrinsic spin-relaxation in molecular magnets on current-induced magnetic switching, Phys. Rev. B **77**, 172414 (2008).

[47] F. Delgado, J. J. Palacios, and J. Fernández-Rossier, Spin-Transfer Torque on a Single Magnetic Adatom, Phys. Rev. Lett. **104**, 026601 (2010).

[48] M. Misiorny and J. Barnaś, Effects of Transverse Magnetic Anisotropy on Current-Induced Spin Switching, Phys. Rev. Lett. **111**, 046603 (2013).

[49] M. Misiorny and I. Weymann, Transverse anisotropy effects on spin-resolved transport through large-spin molecules, Phys. Rev. B **90**, 235409 (2014).

[50] P. Tyagi and E. Friebe, Large resistance change on magnetic tunnel junction based molecular spintronics devices, J. Magn. Magn. Mater. **453**, 186 (2018).

[51] E. Sierda, M. Elsebach, R. Wiesendanger, and M. Bazarnik, Probing weakly hybridized magnetic molecules by single-atom magnetometry, Nano Lett. **19**, 9013 (2019).

[52] B. Verlhac, N. Bachellier, L. Garnier, M. Ormaza, P. Abufager, R. Robles, M.-L. Bocquet, M. Ternes, N. Lorente, and L. Limot, Atomic-scale spin sensing with a single molecule at the apex of a scanning tunneling microscope, Science **366**, 623 (2019).

[53] M. Misiorny, M. Hell, and M. R. Wegewijs, Spintronic magnetic anisotropy, Nat. Phys. **9**, 801 (2013).

[54] J. O. Johansson, J.-W. Kim, E. Allwright, D. M. Rogers, N. Robertson, and J.-Y. Bigot, Directly probing spin dynamics in a molecular magnet with femtosecond time-resolution, Chem. Sci. **7**, 7061 (2016).

[55] K. Katoh, S. Yamashita, N. Yasuda, Y. Kitagawa, B. K. Breedlove, Y. Nakazawa, and M. Yamashita, Control of the spin dynamics of single-molecule magnets by using a quasi one-dimensional arrangement, Angew. Chem. Int. Ed. **57**, 9262 (2018).

[56] G. Taran, E. Bonet, and W. Wernsdorfer, Decoherence measurements in crystals of molecular magnets, Phys. Rev. B **99**, 180408(R) (2019).

[57] D. Roosen, M. R. Wegewijs, and W. Hofstetter, Nonequilibrium Dynamics of Anisotropic Large Spins in the Kondo Regime: Time-Dependent Numerical Renormalization Group Analysis, Phys. Rev. Lett. **100**, 087201 (2008).

[58] A. Płomińska, M. Misiorny, and I. Weymann, Spin-resolved dynamical conductance of a correlated large-spin magnetic molecule, Phys. Rev. B **95**, 155446 (2017).

[59] H. Hammar and J. Fransson, Transient spin dynamics in a single-molecule magnet, Phys. Rev. B **96**, 214401 (2017).

[60] A. Płomińska, I. Weymann, and M. Misiorny, Dynamical spin accumulation in large-spin magnetic molecules, Phys. Rev. B **97**, 035415 (2018).

[61] J. Martinek, Y. Utsumi, H. Imamura, J. Barnaś, S. Maekawa, J. König, and G. Schön, Kondo Effect in Quantum Dots Coupled to Ferromagnetic Leads, Phys. Rev. Lett. **91**, 127203 (2003).

[62] J. Martinek, M. Sindel, L. Borda, J. Barnaś, R. Bulla, J. König, G. Schön, S. Maekawa, and J. von Delft, Gate-controlled spin splitting in quantum dots with ferromagnetic leads in the Kondo regime, Phys. Rev. B **72**, 121302(R) (2005).

[63] J. R. Hauptmann, J. Paaske, and P. E. Lindelof, Electric-field-controlled spin reversal in a quantum dot with ferromagnetic contacts, Nat. Phys. **4**, 373 (2008).

[64] M. Gaass, A. K. Hüttel, K. Kang, I. Weymann, J. von Delft, and Ch. Strunk, Universality of the Kondo Effect in Quantum Dots with Ferromagnetic Leads, Phys. Rev. Lett. **107**, 176808 (2011).

[65] K. P. Wójcik, M. Misiorny, and I. Weymann, Giant superconducting proximity effect on spintronic anisotropy, Phys. Rev. B **100**, 045401 (2019).

[66] G. Taran, E. Bonet, and W. Wernsdorfer, The role of the quadrupolar interaction in the tunneling dynamics of lanthanide molecular magnets, J. Appl. Phys. **125**, 142903 (2019).

[67] K. G. Wilson, The renormalization group: Critical phenomena and the Kondo problem, Rev. Mod. Phys. **47**, 773 (1975).

[68] R. Bulla, T. A. Costi, and T. Pruschke, Numerical renormalization group method for quantum impurity systems, Rev. Mod. Phys. **80**, 395 (2008).

[69] We used the open-access Budapest Flexible DM-NRG code, http://www.phy.bme.hu/~dmnrg/; O. Legeza, C. P. Moca, A. I. Tóth, I. Weymann, and G. Zaránd, Manual for the Flexible DM-NRG code, arXiv:0809.3143.

[70] F. B. Anders and A. Schiller, Real-Time Dynamics in Quantum-Impurity Systems: A Time-Dependent Numerical Renormalization-Group Approach, Phys. Rev. Lett. **95**, 196801 (2005).

[71] F. B. Anders and A. Schiller, Spin precession and real-time dynamics in the Kondo model: Time-dependent numerical renormalization-group study, Phys. Rev. B **74**, 245113 (2006).

[72] H. T. M. Nghiem and T. A. Costi, Generalization of the time-dependent numerical renormalization group method to finite temperatures and general pulses, Phys. Rev. B **89**, 075118 (2014).

[73] H. T. M. Nghiem and T. A. Costi, Time-dependent numerical renormalization group method for multiple quenches: Application to general pulses and periodic driving, Phys. Rev. B **90**, 035129 (2014).

[74] H. T. M. Nghiem and T. A. Costi, Time-dependent numerical renormalization group method for multiple quenches: towards exact results for the long time limit of thermodynamic observables and spectral functions, Phys. Rev. B **98**, 155107 (2018).

[75] M.-S. Choi, D. Sánchez, and R. López, Kondo Effect in a Quantum Dot Coupled to Ferromagnetic Leads: A Numerical Renormalization Group Analysis, Phys. Rev. Lett. **92**, 056601 (2004).

[76] M. Sindel, L. Borda, J. Martinek, R. Bulla, J. König, G. Schön, S. Maekawa, and J. von Delft, Kondo quantum dot coupled to ferromagnetic leads: Numerical renormalization group study, Phys. Rev. B **76**, 045321 (2007).

[77] A. Weichselbaum and J. von Delft, Sum-Rule Conserving Spectral Functions from the Numerical Renormalization Group, Phys. Rev. Lett. **99**, 076402 (2007).

[78] A. Weichselbaum, Tensor networks and the numerical renormalization group, Phys. Rev. B **86**, 245124 (2012).

[79] K. Wrześniewski and I. Weymann, Quench dynamics of spin in quantum dots coupled to spin-polarized leads, Phys. Rev. B **100**, 035404 (2019).

[80] Y. Meir and N. S. Wingreen, Landauer Formula for the Current through an Interacting Electron Region, Phys. Rev. Lett. **68**, 2512 (1992).

[81] M. Yoshida, M. A. Whitaker, and L. N. Oliveira, Renormalization-group calculation of excitation properties for impurity models, Phys. Rev. B **41**, 9403 (1990).